UCRL-JRNL-203522 Version date: April 15, 2004

Poroelastic Fluid Effects on Shear for Rocks with Soft Anisotropy

James G. Berryman
University of California
Lawrence Livermore National Laboratory
P. O. Box 808 L-200
Livermore, CA 94551-9900

Abstract

A general analysis of poroelasticity for vertical transverse isotropy (VTI) shows that four eigenvectors are pure shear modes with no coupling to the pore-fluid mechanics. The remaining two eigenvectors are linear combinations of pure compression and uniaxial shear, both of which are coupled to the fluid mechanics. After reducing the problem to a 2×2 system, the analysis shows in a relatively elementary fashion how a poroelastic system with isotropic solid elastic frame, but with anisotropy introduced through the poroelastic coefficients, interacts with the mechanics of the pore fluid and produces shear dependence on fluid properties in the overall poroelastic system. The analysis shows for example that this effect is always present (though sometimes small in magnitude) in the systems studied, and can be quite large (on the order of 10 to 20%) for wave propagation studies in some real granites and sandstones, including Spirit River sandstone and Schuler-Cotton Valley sandstone. Some of the results quoted here are obtained by using a new product formula relating local bulk and uniaxial shear energy to the product of the two eigenvalues that are coupled to the fluid mechanics. This product formula was first derived in prior work, but is given a more intuitive derivation here. The results obtained here are observed to be useful both for explaining difficult to reconcile experimental data, and for benchmarking of poroelastic codes.

Keywords: porous media, solid-fluid interaction, shear deformation, anisotropic, rock mechanics

1 Introduction

Recent experimental results in ocean sediment acoustics (Williams *et al.*, 2002) tend to show that there are significant discrepancies between Biot's theory (Biot, 1962a,b) and measured poroelastic wave attenuation in the frequency band 2.6-400 kHz. The observed attenuation shows a different frequency dependence and greater overall reduction in wave amplitude than that predicted by the theory. A number of plausible alternative theories has been proposed to reconcile the data but so far none of these effects has been definitively determined to be the true source of these discrepancies. Similarly, a series of experiments on saturated sedimentary rocks by Sams *et al.* (1997) ranging from 30 Hz to 900 kHz has shown that the theory can be used to fit these seismic, well-logging, and laboratory ultrasonic data. But in order to do so, Biot's theory must be supplemented with some additional mechanisms to explain fully the poroelastic velocity dispersion and wave attenuation observed. Again the data available are not yet sufficient to help us distinguish with certainty what the precise cause of these significant variations of the data with frequency might be.

There have been many proposals made that supply physically reasonable mechanisms resulting in greater dispersion and attenuation in field data, but it is beyond our purpose and scope to review these here. The point to be made instead is that the measured effects are clearly multiscale phenomena, and they are usually not treated as such [but see Pride *et al.* (2004) for one exception]. Biot's theory is a relatively simple one for the complex systems considered. For fundamental reasons required to produce such a simple phenomenological theory, Biot necessarily assumes that the medium has constant porosity and is microhomogeneous, linear, usually isotropic, etc. Virtually all of these fundamental requirements of the theory are often violated in the earth for the applications of interest. Nevertheless, it is known that ultrasonic data

(Plona, 1980) on samples of sintered glass beads — and satisfying all Biot's assumptions — can be reconciled with the theory in detail (Chin *et al.*, 1985; Bourbié *et al.*, 1987), including wave speeds, attenuation, and the predicted existence of a second compressional wave. So, it is the present author's working hypothesis that the underlying reason for the observed discrepancies, in all cases involving earth materials, is heterogeneity, or anisotropy, or some combination of the two.

In recent papers (Berryman, 2004a,c), the author has addressed the issue of earth heterogeneity in this context and shown how a layered earth affects the overall shear modulus of such a system. An important outcome of this work is a rigorous product formula (given a new derivation here in an Appendix), valid for any transversely isotropic poroelastic medium, and showing how the compressional and shear moduli are coupled under undrained conditions. Such undrained conditions are typically studied in poroelastic wave problems as a proxy for the more difficult problem of understanding exactly how the system behaves at high frequencies, *i.e.*, sufficiently high that the fluid is essentially confined (some authors use the term "unrelaxed" in this context) during the time of wave passage. We will also study the undrained shear modulus in the present contribution, but no layering will be assumed — so we may separate out the contributions of heterogeneity from those of anisotropy. In fact we find that the contributions from heterogeneity and anisotropy are very similar in these systems. This is due in part, of course, to the fact that locally layered heterogeneity also leads to effective overall anisotropy.

A brief history of the theory on this topic is this: An important paper by Gassmann (1951) concerns the effects of fluids on the mechanical properties of porous rock. His main result is the well-known fluid-substitution formula (that now bears his name) for the bulk modulus in undrained, isotropic poroelastic media. He also postulated that the effective undrained shear modulus would (in contrast to the bulk modulus) be independent of the mechanical properties of the fluid when the medium is isotropic. That the independence of shear modulus from fluid effects is guaranteed for isotropic media at very low or quasistatic frequencies was shown recently by Berryman (1999) to be tightly coupled to the original bulk modulus result of Gassmann; each result implies the other in isotropic media. [Note that a recently discovered product formula (Berryman, 2004a) suggests that there is also a similarly tight coupling between the modes for heterogeneous and anisotropic systems, as will be elaborated upon here.] It has gone mostly without discussion in the literature that Gassmann (1951) also derived general results for anisotropic porous rocks in the same 1951 paper. It is not hard to see that these results imply that, contrary to the isotropic case, some of the overall *undrained* shear moduli in fact may depend on fluid properties in anisotropic media, thus mimicking the bulk modulus behavior. However, Gassmann's paper does not remark at all on this difference in behavior between isotropic and anisotropic porous rocks. Brown and Korringa (1975) also address the same class of problems, including both isotropic and anisotropic cases, but again they do not remark on the shear modulus results in either case. Norris (1993) studies partial saturation in isotropic layered materials in the low-frequency regime ($\simeq$ 100 Hz) and takes as a fundamental postulate that Gassmann's results hold for the low frequency shear modulus, but it seems that some more justification should be provided for such an assumption, and furthermore some indication of its range of validity established.

On the other hand, Hudson (1981), in his early work on cracked solids, explicitly demonstrates differences between fluid-saturated and dry cracks and relates his work to that of Walsh (1969) and O'Connell and Budiansky (1974), but does not make any connection to the work

of Gassmann (1951), Biot and Willis (1957), or Brown and Korringa (1975). Mukerji and Mavko (1994) show numerical results based on work of Gassmann (1951), Brown and Korringa (1975) and Hudson (1981) demonstrating the fluid dependence of shear in anisotropic rock, but again they do not remark on these results at all. Mavko and Jizba (1991) use a rather simple reciprocity argument to establish a direct, but approximate, connection between undrained shear response and undrained compressional response in rocks containing cracks. Berryman and Wang (2001) show that deviations from Gassmann's results sufficient to produce shear modulus dependence on fluid mechanical properties require the presence of some anisotropy on the microscale, thereby explicitly violating the microhomogeneous and microisotropy conditions implicit in Gassmann's original derivation. Berryman *et al.* (2002a) go further and make use of differential effective medium analysis to show explicitly how the undrained, overall isotropic shear modulus can depend on fluid trapped in penny-shaped cracks. Meanwhile, laboratory results for wave propagation [see Berryman *et al.* (2002b)] show conclusively that the shear modulus does indeed depend on fluid mechanical properties for low-porosity, low-permeability rocks, and high-frequency laboratory experiments ($f > 500$ kHz).

One thing lacking from all the preceding work is a simple example showing how the presence of anisotropy influences the shear modulus, and specifically when and how the shear modulus becomes fluid dependent. Our main purpose in the present work is therefore to demonstrate, in a set of quite simple examples, how the overall shear behavior becomes coupled to fluid compressional properties at high frequencies in anisotropic media — even though overall shear modulus is always independent of the fluid properties in microhomogeneous isotropic media at sufficiently low frequencies, whether drained or undrained. Two other distinct but related analyses addressing this topic have been presented recently by the author (Berryman, 2004a,c). Both of these prior papers have made explicit use of layered media, composed of isotropic poroelastic materials, together with exact results for such media based on low frequency, long wavelength Backus averaging (Backus, 1962). In contrast, the present analysis does *not* make use of such a specific model, and is therefore believed to be about as simple as possible, while still achieving the level of understanding desired for this rather subtle technical issue. One important simplification we make here in order to separate the part that is due to poroelastic effects from the part that would be present in any elastic (*i.e.*, possibly zero permeability porous medium) is to model each material as if the elastic part is entirely isotropic, while the poroelastic effects [*i.e.*, the effective stress or Biot-Willis coefficients (Biot and Willis, 1957) for the anisotropic overall material] provide the only sources of anisotropy in the system. Thus, we specifically distinguish two possible sources of anisotropy, the elastic or "hard" anisotropy that is assumed not to be present here, and the poroelastic or "soft" anisotropy that is the source of the effects we want to study in this paper.

Our analysis for general transversely isotropic media is presented in Sections 2–4. To be specific, Section 4 also introduces the effective undrained shear modulus relevant to our general discussion. Examples are presented for glass, granite, and two sandstones in Section 5. The paper's results and conclusions are summarized in the final section. Some mathematical details are collected in two Appendices. In particular, a new derivation of the product formula that is key to our analysis is presented in Appendix B.

2 Fluid-Saturated Poroelastic Rocks

In contrast to traditional elastic analysis, the presence in rock of a saturating pore fluid introduces the possibility of an additional control field and an additional type of strain variable. The pressure p_f in the fluid is a new field parameter that can be controlled. Allowing sufficient time for global pressure equilibration permits us to consider p_f to be a constant throughout the percolating (connected) pore fluid, while restricting the analysis to quasistatic processes. (But ultimately we are not interested in such quasi-static processes in this paper, as we are trying to reconcile laboratory wave data with the theory.) The change ζ in the amount of fluid mass contained in the pores [see Biot (1962) or Berryman and Thigpen (1985)] is a new type of strain variable, measuring how much of the original fluid in the pores is squeezed out during the compression of the pore volume while including the effects of compression or expansion of the pore fluid itself due to changes in p_f. It is most convenient to write the resulting equations in terms of compliances rather than stiffnesses, so the basic equation to be considered takes the following form for isotropic media:

$$\begin{pmatrix} e_{11} \\ e_{22} \\ e_{33} \\ -\zeta \end{pmatrix} = \begin{pmatrix} s_{11} & s_{12} & s_{12} & -\beta \\ s_{12} & s_{11} & s_{12} & -\beta \\ s_{12} & s_{12} & s_{11} & -\beta \\ -\beta & -\beta & -\beta & \gamma \end{pmatrix} \begin{pmatrix} \sigma_{11} \\ \sigma_{22} \\ \sigma_{33} \\ -p_f \end{pmatrix}. \tag{1}$$

The constants appearing in the matrix on the right hand side will be defined in the following two paragraphs. It is important to write the equations this way rather than using the inverse relation in terms of the stiffnesses, because the compliances s_{ij} appearing in (1) are simply related to the drained elastic constants λ_{dr} and G_{dr} in the same way they are related in normal elasticity, whereas the individual stiffnesses obtained by inverting the equation in (1) must contain coupling terms through the parameters β and γ that depend on the pore and fluid compliances. Thus, we find that

$$s_{11} = \frac{1}{E_{dr}} = \frac{\lambda_{dr} + G_{dr}}{G_{dr}(3\lambda_{dr} + 2G_{dr})} \tag{2}$$

and

$$s_{12} = -\frac{\nu_{dr}}{E_{dr}}, \tag{3}$$

where the drained Young's modulus E_{dr} is defined by the second equality of (2) and the drained Poisson's ratio is determined by

$$\nu_{dr} = \frac{\lambda_{dr}}{2(\lambda_{dr} + G_{dr})}. \tag{4}$$

When the external stress is hydrostatic so $\sigma = \sigma_{11} = \sigma_{22} = \sigma_{33}$, equation (1) telescopes down to

$$\begin{pmatrix} e \\ -\zeta \end{pmatrix} = \begin{pmatrix} 1/K_{dr} & -\alpha/K_{dr} \\ -\alpha/K_{dr} & \alpha/BK_{dr} \end{pmatrix} \begin{pmatrix} \sigma \\ -p_f \end{pmatrix}, \tag{5}$$

where $e = e_{11} + e_{22} + e_{33}$, $K_{dr} = \lambda_{dr} + \frac{2}{3}G_{dr}$ is the drained bulk modulus, $\alpha = 1 - K_{dr}/K_m$ is the Biot-Willis parameter (Biot and Willis, 1957) with K_m being the bulk modulus of the

solid minerals present, and Skempton's pore-pressure buildup parameter B (Skempton, 1954) is given by

$$B = \frac{1}{1 + K_p(1/K_f - 1/K_m)}. \tag{6}$$

New parameters appearing in (6) are the bulk modulus of the pore fluid K_f and the pore modulus $K_p^{-1} = \alpha/\phi K_{dr}$ where ϕ is the porosity. The expressions for α and B can be generalized slightly by supposing that the solid frame is composed of more than one constituent, in which case the K_m appearing in the definition of α is replaced by K_s and the K_m appearing explicitly in (6) is replaced by K_ϕ (see Brown and Korringa, 1975; Rice and Cleary, 1976; Berryman and Wang, 1995). This is an important additional complication (Berge and Berryman, 1995), but — for the sake of desired simplicity — we will not pursue the matter further here.

Comparing (1) and (5), we find that

$$\beta = \frac{\alpha}{3K_{dr}} \tag{7}$$

and

$$\gamma = \frac{\alpha}{BK_{dr}}. \tag{8}$$

As we develop the ideas to be presented here, we will need to treat Eqs. (1)–(6) as if they are true locally, but perhaps not globally. In particular, if we assume overall drained conditions, then p_f = a constant everywhere. But, if we assume locally undrained conditions, then $p_f \simeq$ a constant in local patches, but these local constant values may differ from patch to patch. This way of thinking about the system is intended to mimic the behavior expected when a high frequency wave propagates through a system having highly variable (or just uniformly very low) fluid permeability everywhere.

3 Relations for Anisotropy in Poroelastic Materials

Gassmann (1951), Brown and Korringa (1975), and others have considered the problem of obtaining effective constants for anisotropic poroelastic materials when the pore fluid is confined within the pores. The confinement condition amounts to a constraint that the increment of fluid content $\zeta = 0$, while the external loading σ is changed and the pore-fluid pressure p_f is allowed to respond as necessary and thus equilibrate.

To provide an elementary derivation of the Gassmann equation for anisotropic materials, we consider the anisotropic generalization of (1)

$$\begin{pmatrix} e_{11} \\ e_{22} \\ e_{33} \\ -\zeta \end{pmatrix} = \begin{pmatrix} s_{11} & s_{12} & s_{13} & -\beta_1 \\ s_{12} & s_{22} & s_{23} & -\beta_2 \\ s_{13} & s_{23} & s_{33} & -\beta_3 \\ -\beta_1 & -\beta_2 & -\beta_3 & \gamma \end{pmatrix} \begin{pmatrix} \sigma_{11} \\ \sigma_{22} \\ \sigma_{33} \\ -p_f \end{pmatrix}. \tag{9}$$

Three shear contributions have been excluded from consideration since they can easily be shown not to interact mechanically with the fluid effects. This form is not completely general in that

it includes orthorhombic, cubic, hexagonal, and all isotropic systems, but excludes triclinic, monoclinic, trigonal, and some tetragonal systems that would have some nonzero off-diagonal terms in the full elastic matrix. Also, we have assumed that the material axes are aligned with the spatial axes. But this latter assumption is not significant for the derivation that follows. Such an assumption is important when properties of laminated materials having arbitrary orientation relative to the spatial axes need to be considered, but we do not treat this more general problem here.

If the fluid is confined (or undrained on the time scales of interest), then $\zeta \equiv 0$ in (9) and p_f becomes a linear function of σ_{11}, σ_{22}, σ_{33}. Eliminating p_f from the resulting equations, we obtain the general expression for the strain dependence on external stress under confined conditions:

$$\begin{pmatrix} e_{11} \\ e_{22} \\ e_{33} \end{pmatrix} = \left[\begin{pmatrix} s_{11} & s_{12} & s_{13} \\ s_{12} & s_{22} & s_{23} \\ s_{13} & s_{23} & s_{33} \end{pmatrix} - \gamma^{-1} \begin{pmatrix} \beta_1 \\ \beta_2 \\ \beta_3 \end{pmatrix} (\beta_1 \quad \beta_2 \quad \beta_3) \right] \begin{pmatrix} \sigma_{11} \\ \sigma_{22} \\ \sigma_{33} \end{pmatrix}$$

$$\equiv \begin{pmatrix} s^*_{11} & s^*_{12} & s^*_{13} \\ s^*_{12} & s^*_{22} & s^*_{23} \\ s^*_{13} & s^*_{23} & s^*_{33} \end{pmatrix} \begin{pmatrix} \sigma_{11} \\ \sigma_{22} \\ \sigma_{33} \end{pmatrix}. \tag{10}$$

The s_{ij}'s are fluid-drained constants, while the s^*_{ij}'s are the fluid-undrained (or fluid-confined) constants.

The fundamental result (10) was obtained earlier by both Gassmann (1951) and Brown and Korringa (1975), and may be written simply as

$$s^*_{ij} = s_{ij} - \frac{\beta_i \beta_j}{\gamma}, \quad \text{for} \quad i, j = 1, 2, 3. \tag{11}$$

This expression is just the anisotropic generalization of the well-known Gassmann equation for isotropic, microhomogeneous porous media.

4 Eigenvectors for Transverse Isotropy

The 3×3 system (10) can be analyzed fairly easily, and in particular the eigenfunctions and eigenvalues of this system can be obtained in general. However, such general results do not provide much physical insight into the problem we are trying to study, so instead of proceeding in this direction we will now restrict attention to transversely isotropic materials. This case is relevant to many layered earth materials and also industrial systems, and it is convenient because we can immediately eliminate one of the eigenvectors from further consideration. Three mutually orthogonal (but unnormalized) vectors of interest are:

$$v_1 = \begin{pmatrix} 1 \\ 1 \\ 1 \end{pmatrix}, \qquad v_2 = \begin{pmatrix} 1 \\ -1 \\ 0 \end{pmatrix}, \qquad v_3 = \begin{pmatrix} 1 \\ 1 \\ -2 \end{pmatrix}. \tag{12}$$

Treating these vectors as stresses, the first corresponds to a simple hydrostatic stress, the second to a planar shear stress, and the third to a pure shear stress applied uniaxially along the z-axis (which would also be the symmetry axis for a layered system, but we are not treating such

layered systems here). Transverse isotropy of the layered system requires: $s_{11} = s_{22}$, $s_{13} = s_{23}$, and for the poroelastic problem $\beta_1 = \beta_2$. Thus, it is immediately apparent that the planar shear stress v_2 is an eigenvector of the system, and furthermore it results in no contribution from the pore fluid. Therefore, this vector will be of no further interest here, and the system can thereby be reduced to 2×2.

4.1 Compliance formulation

If we define the effective compliance matrix for the system as S^* having the matrix elements given in (11), then the bulk modulus for this system is defined in terms of v_1 by

$$\frac{1}{K_u} = v_1^T S^* v_1 = \frac{1}{K_{dr}} - \gamma^{-1} \left(2\beta_1 + \beta_3\right)^2, \tag{13}$$

where the T superscript indicates the transpose, and $1/K_{dr} \equiv \sum_{i,j=1}^{3} s_{ij}$. This is the result usually quoted as Gassmann's equation for the bulk modulus of the undrained (or confined) anisotropic (VTI) system. Also, note that in general

$$\sum_{i=1}^{3} \beta_i = 2\beta_1 + \beta_3 = \alpha/K_{dr}. \tag{14}$$

Thus, even though v_1 is not an eigenvector of this system, it nevertheless plays a fundamental role in the mechanics. Furthermore, this role is quite well-understood. What is perhaps not as well-understood then, especially for poroelastic systems, is the role of v_3. Understanding this role will be one main focus for the remainder of this discussion.

The true eigenvectors of the subproblem of interest (*i.e.*, in the space orthogonal to the four pure shear eigenvectors already discussed) are necessarily linear combinations of v_1 and v_3. We can construct the relevant contracted operator for the 2×2 subsystem by considering:

$$\begin{pmatrix} v_1^T \\ v_3^T \end{pmatrix} S^* \begin{pmatrix} v_1 & v_3 \end{pmatrix} \equiv \begin{pmatrix} 9A_{11}^* & 18A_{13}^* \\ 18A_{13}^* & 36A_{33}^* \end{pmatrix} \tag{15}$$

(in all cases the $*$ superscripts indicate that the pore-fluid effects are included) and the reduced matrix

$$\Sigma^* = A_{11}^* v_1 v_1^T + A_{13}^* (v_1 v_3^T + v_3 v_1^T) + A_{33}^* v_3 v_3^T, \tag{16}$$

where

$$\begin{aligned} A_{11}^* &= [2(s_{11}^* + s_{12}^* + 2s_{13}^*) + s_{33}^*]/9, \\ A_{13}^* &= (s_{11}^* + s_{12}^* - s_{13}^* - s_{33}^*)/9, \\ A_{33}^* &= (s_{11}^* + s_{12}^* - 4s_{13}^* + 2s_{33}^*)/18. \end{aligned} \tag{17}$$

Providing some understanding of these connections and the implications for shear modulus dependence on fluid content is one of our goals.

First we remark that $A_{11}^* = 1/9K_u$, where K_u is again the undrained (or Gassmann) bulk modulus for the system in (13). Therefore, A_{11}^* is proportional to the undrained bulk compliance

of this system. The other two matrix elements cannot be given such simple interpretations in general. To simplify the analysis we note that, at least for purposes of modeling, anisotropy of the compliances s_{ij} and the poroelastic coefficients β_i can be treated independently. Anisotropy displayed in the s_{ij}'s corresponds mostly to the anisotropy in the solid elastic components of the system, while anisotropy in the β_i's corresponds mostly to anisotropy in the shapes and spatial distribution of the porosity. We will therefore distinguish these contributions by calling anisotropy appearing in the s_{ij}'s the "hard anisotropy," and the anisotropy in the β_i's will in contrast be called the "soft anisotropy."

Now, it is clear (also see the discussion in Appendix A for more details) that the eigenvectors having unit magnitude $f(\theta)$ for this problem (*i.e.*, for the reduced operator Σ^*) necessarily take the form

$$f(\theta) = \overline{v}_1 \cos\theta + \overline{v}_3 \sin\theta, \tag{18}$$

where $\overline{v}_1 = v_1/\sqrt{3}$ and $\overline{v}_3 = v_3/\sqrt{6}$ are the normalized basis vectors. The 2×2 system must have two eigenvectors, corresponding two angles we label θ_+ and θ_- (for the $\pm$ signs appearing in the quadratic forms that appear in the eigenvalue formulas). Furthermore, the orthogonality condition for the eigenvectors is

$$0 = f^T(\theta_+) f(\theta_-) = \cos\theta_+ \cos\theta_- + \sin\theta_+ \sin\theta_- = \cos(\theta_+ - \theta_-), \tag{19}$$

which implies that the difference $\theta_+ - \theta_- = \pm\pi/2$. The two solutions for the rotation angle, when chosen appropriately, may therefore be related by: θ_+ and $\theta_- = \theta_+ + \frac{\pi}{2}$. It is easily seen that the eigenvalues are given by

$$\Lambda^*_\pm = 3\left[A^*_{33} + A^*_{11}/2 \pm \sqrt{(A^*_{33} - A^*_{11}/2)^2 + 2(A^*_{13})^2}\right] \tag{20}$$

and the rotation angles are determined by

$$\tan\theta^*_\pm = \frac{\Lambda^*_\pm/3 - A^*_{11}}{\sqrt{2}A^*_{13}} = \left[A^*_{33} - A^*_{11}/2 \pm \sqrt{(A^*_{33} - A^*_{11}/2)^2 + 2(A^*_{13})^2}\right]/\sqrt{2}A^*_{13}. \tag{21}$$

One part of the rotation angle is due to the drained (fluid free) "hard anisotropic" nature of the rock frame material. We will call this part $\bar{\theta}$. The remainder is due to the presence of the fluid in the pores, and we will call this part $\delta\theta \equiv \theta^* - \bar{\theta}$ for the "soft anisotropy." Using a standard formula for tangents, we have

$$\delta\theta_\pm = \tan^{-1}\left[\frac{\tan\theta^*_\pm - \tan\bar{\theta}_\pm}{1 + \tan\theta^*_\pm \tan\bar{\theta}_\pm}\right]. \tag{22}$$

Furthermore, definite formulas for $\bar{\theta}_\pm$ are found from (21) by taking $\gamma \to \infty$ (corresponding to air saturation of the pores).

Since (19) implies that

$$\tan\theta^*_+ \cdot \tan\theta^*_- = -1, \tag{23}$$

it is sufficient to consider just one of the signs in front of the radical in (21). The most convenient choice for analytical purposes turns out to be the minus sign (which corresponds to

the eigenvector with the larger component of pure compression). Furthermore, it is also clear from the form of (21) that often the behavior of most interest to us here occurs for cases when $A^*_{13} \neq 0$.

In the limit of a nearly isotropic solid frame (so the "hard anisotropy" vanishes and thus we will also call this the "quasi-isotropic" limit), it is not hard to see that

$$A^*_{33} \simeq \frac{1}{12G_{dr}} - \frac{(\beta_1 - \beta_3)^2}{9\gamma}, \tag{24}$$

where G_{dr} is the drained shear modulus of the quasi-isotropic solid frame. Similarly, the remaining coefficient

$$A^*_{13} \simeq -\frac{(\beta_1 - \beta_3)(2\beta_1 + \beta_3)}{9\gamma}, \tag{25}$$

since all the solid contributions approximately cancel in this limit.

To clarify the situation further, we will enumerate three cases:

4.1.1 *Case I.* $A^*_{33} - A^*_{11}/2 \neq 0$, $A^*_{13} = 0$.

Whenever $A^*_{33} - A^*_{11}/2 \neq 0$ and $A^*_{13} \to 0$, we find easily that $\theta^*_- \to 0$, while $\theta^*_+ \to \pi/2$. In this case, v_1 and v_3 are themselves the eigenvectors, while the eigenvalues are proportional to A^*_{11} and A^*_{33}. In the quasi-isotropic limit, A^*_{13} can vanish only if $\beta_1 - \beta_3 = 0$, in which case A^*_{33} also does not depend on fluid properties. For media differing significantly from the quasi-isotropic limit, A^*_{13} could vanish for some physically interesting situations, but the resulting physical constraints are too special (and complicated) for us to consider them further here.

4.1.2 *Case II.* $A^*_{33} - A^*_{11}/2 = 0$, $A^*_{13} \neq 0$.

For this case, $\tan\theta^*_\pm = \pm 1$, so $\theta^*_\pm = \pm\pi/4$. The two eigenvectors are $v_1/\sqrt{6} \pm v_3/\sqrt{12}$, with no dependence on the fluid properties. However, the eigenvalues continue to be functions of the fluid properties. This seems to be a rather special case, but again considering the quasi-isotropic limit, we find that $A^*_{33} - A^*_{11}/2 \simeq \nu/2E + [(2\beta_1 + \beta_3)^2 - 2(\beta_1 - \beta_3)^2]/18\gamma$, where ν is Poisson's ratio and E is Young's modulus. For this combination of the parameters to vanish for special values does not appear to violate any of the well-known constraints (such as positivity, etc.) on these parameters. For example, if $\beta_1 = 0$, the term depending on the fluid properties clearly makes a negative contribution, which might be large enough to cancel the contribution from the solid. But, for now, this case seems rather artificial, so we will not consider it further here.

4.1.3 *Case III.* $A^*_{33} - A^*_{11}/2 \neq 0$, $A^*_{13} \neq 0$.

This case is the most general one of the three, and the one we will study at greater length in the remainder of this discussion.

We want to understand how the introduction of liquid into the pore space affects the shear modulus. We also want to know how the anisotropy influences, *i.e.*, aids or hinders, the impact of the liquid on the shear behavior. To achieve this understanding, it should be sufficient to

consider the case when $(A^*_{13})^2 \ll (A^*_{33} - A^*_{11}/2)^2$, assuming as we do that both factors are nonzero. Then, expanding the square root in (20), we have

$$\Lambda^*_+ = 6A^*_{33} + \Delta \quad \text{and} \quad \Lambda^*_- = 3A^*_{11} - \Delta, \tag{26}$$

where Δ is defined consistently by either of the two preceeding expressions or by $2\Delta \equiv \Lambda^*_+ - \Lambda^*_- + 3A_{11} - 6A_{33}$ and is also given approximately for cases of interest here by

$$\Delta \simeq \frac{3(A^*_{13})^2}{A^*_{33} - A^*_{11}/2}. \tag{27}$$

In the quasi-isotropic soft anisotropy limit under consideration, we find

$$\Delta \simeq \frac{2(\beta_1 - \beta_3)^2(2\beta_1 + \beta_3)^2/27\gamma^2}{\nu/E + [(2\beta_1 + \beta_3)^2 - 2(\beta_1 - \beta_3)^2]/9\gamma}. \tag{28}$$

All of the mechanical effects of the liquid that contribute to this formula appear in the factor γ. The order at which γ appears depends on the relative importance of the two terms in the denominator of this expression. If the second term ever dominates, then one factor of γ cancels, and therefore $\Delta \sim O(\gamma^{-1})$, and furthermore $\Delta \sim 2(\beta_1 - \beta_3)^2/3\gamma$ if $|\beta_1 - \beta_3| << |2\beta_1 + \beta_3|$. If instead what seems to be the more likely situation holds and the first term in the denominator dominates, then $\Delta \sim O(\gamma^{-2})$. So in either of these cases, as long as $\beta_1 - \beta_3 \neq 0$ (which is the condition for soft anisotropy), we always have contributions to Δ from liquid mechanical effects. There do not appear to be any combinations of the parameters for which the fluid effects disappear whenever the material is in the class of anisotropic solids considered here.

4.2 Stiffness formulation

The dual to the problem just studied replaces compliances everywhere with stiffnesses, and then proceeds as before. Equations (15)–(18) are replaced by

$$\begin{pmatrix} v_1^T \\ v_3^T \end{pmatrix} C^* \begin{pmatrix} v_1 & v_3 \end{pmatrix} \equiv \begin{pmatrix} 9B^*_{11} & 18B^*_{13} \\ 18B^*_{13} & 36B^*_{33} \end{pmatrix} \tag{29}$$

(in all cases the $*$ superscripts indicate that the pore-fluid effects are included) and the reduced matrix

$$(\Sigma^*)^{-1} = B^*_{11} v_1 v_1^T + B^*_{13}(v_1 v_3^T + v_3 v_1^T) + B^*_{33} v_3 v_3^T, \tag{30}$$

where

$$\begin{aligned} B^*_{11} &= [2(c^*_{11} + c^*_{12} + 2c^*_{13}) + c^*_{33}]/9, \\ B^*_{13} &= (c^*_{11} + c^*_{12} - c^*_{13} - c^*_{33})/9, \\ B^*_{33} &= (c^*_{11} + c^*_{12} - 4c^*_{13} + 2c^*_{33})/18. \end{aligned} \tag{31}$$

It is a straightforward exercise to check that the two reduced problems are in fact inverses of each other. We will not repeat this analysis here, as it is wholly repetitive of what has gone before. The main difference in the details is that the expressions for the B's in terms of the β's are rather more complicated than those for the compliance version, which is also why we chose to display the compliance formulation instead.

4.3 Effective and undrained shear moduli G_{eff} and G_u

Four shear moduli are easily defined for the anisotropic system under study. Furthermore, since we are treating only soft anisotropy, all of these moduli are the same, *i.e.*, $G_i = G_{dr}$ for $i = 1, \ldots, 4$. These moduli are related to the four shear eigenvalues/eigenvectors of the system, and they do not couple to the pore-fluid mechanics. But, the eigenvectors in the reduced 2×2 system studied here are usually mixed in character, being quasi-compressional or quasi-shear modes. It is therefore somewhat problematic to find a proper definition for a fifth shear modulus. The author has analyzed this problem previously (Berryman, 2004b), and concluded that a sensible (though approximate) definition can be made using $G_5 = G_{eff}$. There are several different ways of arriving at the same result, but for the present analysis the most useful of these is to express G_{eff} in terms of the product $\Lambda_+\Lambda_-$ (the eigenvalue product, which is also the determinant of the 2×2 compliance system). This result is given a new derivation in Appendix B, and for our present application states that the product formula is

$$\frac{1}{3K_u} \cdot \frac{1}{2G_{eff}} \equiv \Lambda_+\Lambda_- = 18 \left[A_{11}^* A_{33}^* - (A_{13}^*)^2 \right], \tag{32}$$

which we take as the definition of G_{eff} here. And, since $A_{11}^* = 1/9K_u$, we have

$$\frac{1}{G_{eff}} = 12 \left[A_{33}^* - (A_{13}^*)^2 / A_{11}^* \right]. \tag{33}$$

To obtain one possible choice for an estimate of the isotropic average overall undrained shear modulus, we next take the arithmetic mean of these five shear compliances:

$$\frac{1}{G_u} \equiv \frac{1}{5} \sum_{i=1}^{5} \frac{1}{G_i}. \tag{34}$$

Combining these definitions and results gives:

$$\frac{1}{G_u} - \frac{1}{G_{dr}} = -\frac{4}{15} \frac{(\beta_1' - \beta_3')^2}{1 - \alpha B} \frac{\alpha B}{K_{dr}} = \frac{4}{15} \frac{(\beta_1' - \beta_3')^2}{1 - \alpha B} \left[\frac{1}{K_u} - \frac{1}{K_{dr}} \right], \tag{35}$$

where the β's are defined by $\beta_i' = \beta_i K_{dr}/\alpha$. The final equality is presented to emphasize the similarity of the present results to those of both Mavko and Jizba (1991) and Berryman *et al.* (2002b). Setting $\beta_1' = 0$, $\beta_3' = 1$, $B = 1$, and $\alpha \simeq 0$ recovers the form of Mavko and Jizba (1991) for the case of a very dilute system of flat cracks. The Mavko-Jizba form was used successfully by Sams *et al.* (1997) while reconciling their high frequency data with the theory.

Note that (34) takes the form of a Reuss-type average (harmonic mean, and lower bound) of the undrained shear modulus. Also note that, contrary to (34), the definition (33) of G_{eff} is actually based instead on the Voigt average. In terms of mathematical precision, the result (35) therefore cannot be considered strictly rigorous; it is neither an upper nor a lower bound. A partial justification for the formula comes not from absolute rigor, but instead from observations (some of which are presented in the next section) that G_{eff} is in fact a very close estimate of the energy per unit volume in the fifth shear mode (though still an upper bound). So, for these reasons, the result (35) should be viewed, not as a rigorous formula (it is not), but as a good physical estimate of the undrained shear modulus. Berryman *et al.* (2002b) show that the Mavko and Jizba (1991) results suffer from the same lack of rigor.

For applications in which rigor is demanded, we should instead use the Voigt average

$$G_u \equiv \frac{1}{5}\sum_i G_i, \tag{36}$$

as our estimate of the effective undrained shear modulus. Berryman (2004a) shows that this choice is often a very accurate estimate, although strictly speaking it should still be viewed as an upper bound on the overall modulus for a random, heterogeneous, anisotropic system.

5 Examples and Discussion

It is clear from (26) that fluid effects in Δ cannot increase the overall compliance eigenvalues simultaneously for both the quasi-bulk and the quasi-shear modes. Rather, if one increases, the other must decrease. Furthermore, it is certainly always true that the presence of pore liquid either has no effect or else strengthens (*i.e.*, stiffens) the porous medium in compression. But this effect on the bulk modulus has been at least partially accounted for in $A_{11}^* = 1/9K^*$ through the original contribution derived by Gassmann (1951). So presumably the contribution of Δ to compliance cannot be so large as to negate completely the liquid effects on the undrained bulk modulus.

5.1 Examples

To clarify the situation, we show some examples in Figures 1–8. The details of the analysis that produces these constant energy ellipses are summarized in Appendix A. The main point is that, for the compliance version of the analysis, the contours of constant energy are ellipses when the vector f in (18) is interpreted as a stress. Analogously, when the vector is treated as a strain, the contours of constant energy are ellipses for the dual (or stiffness) formulation. If we choose to think of these figures as diagrams in the complex plane, then we note that — while circles and lines transform to circles and lines when transforming back and forth between these two planes — the shapes of ellipses are not preserved (except, of course, in the special case – which is precisely that of isotropy – when the ellipses degenerate to circles). Eigenvectors are determined by the directions in which the points of contact of these two curves lie (indicated by red circles).

Figures 1 and 2 present an example based on a glassy material. Typical values for the bulk and shear moduli of glass were used: $K_m = 46.3$ GPa and $G_m = 30.5$ GPa, respectively. The value of the Biot-Willis coefficient was arbitrarily chosen as $\alpha = 0.6$, so $K_{dr} = 18.52$ GPa. Taking Poisson's ratio as $\nu_{dr} = 0.2$, we have $G_{dr} = 13.89$ GPa. Skempton's coefficient was chosen for simplicity to be $B \equiv 1$ in this and all the other examples as well. (This choice is extreme because it implies that $K_u = K_m$. But, since our interest here is in analysis of the undrained shear modulus, the study of this limit is particularly useful to us.) The most anisotropic choices of β_1 and β_3 were used that would not produce absurd (negative) values of the diagonal coefficients for either s_{ij}^* or c_{ij}^*, and that also would not produce $G_u > G_m$. [G_u determined by (33) amd (34) is a type of upper bound – actually the Voigt average. Values of this bound that might exceed G_m need not be considered.] For glass, these values were found to be $\beta_1 = 0.15\alpha/K_{dr}$ and $\beta_3 = 0.70\alpha/K_{dr}$. The value of the energy used for normalization

was $U = 900.0$ GPa. Computed values for the effective and undrained shear moduli were $G_{eff} = 25.43$ GPa and $G_u = 15.28$ GPa.

For the remaining three sets of examples, the values used for the moduli of the samples are taken from results contained in Berryman (2004a), wherein it was shown how certain laboratory data could be fit using an elastic differential effective medium scheme. These results are summarized in the TABLE.

Figures 3 and 4 present results for Sierra White granite. Laboratory data on this material were presented by Murphy (1982). The values chosen for β_1 and β_3 were $\beta_1 = 0.05\alpha/K_{dr}$ and $\beta_3 = 0.90\alpha/K_{dr}$. The value of the energy used for normalization was $U \simeq 900.0$ GPa. Computed values for the effective and undrained shear moduli were $G_{eff} = 39.8$ GPa and $G_u = 28.3$ GPa.

Figures 5 and 6 present results for Schuler-Cotton Valley sandstone. Laboratory data on this material were also presented by Murphy (1982). The values chosen for β_1 and β_3 were $\beta_1 = 0.20\alpha/K_{dr}$ and $\beta_3 = 0.60\alpha/K_{dr}$. The value of the energy used for normalization was $U \simeq 900.0$ GPa. Computed values for the effective and undrained shear moduli were $G_{eff} = 35.8$ GPa and $G_u = 17.7$ GPa.

Figures 7 and 8 present results for Spirit River sandstone. Laboratory data on this material were presented by Knight and Nolen-Hoeksema (1990). The values chosen for β_1 and β_3 were $\beta_1 = 0.25\alpha/K_{dr}$ and $\beta_3 = 0.50\alpha/K_{dr}$. The value of the energy used for normalization was $U \simeq 900.0$ GPa. Computed values for the effective and undrained shear moduli were $G_{eff} = 20.11$ GPa and $G_u = 12.41$ GPa.

5.2 Discussion

We can compare the results obtained with results obtained for the same rocks using differential effective medium theory to fit data. The two characteristics that will interest us here are: (1) comparisons between the values chosen in our examples for the anisotropic β's and the best fitting crack aspect ratios found in Berryman (2004a), and (2) comparisons between the magnitudes of changes in the overall shear moduli from their drained to undrained values.

The preferred crack aspect ratios found for Sierra White granite, Schuler-Cotton Valley sandstone, and Spirit River sandstone in Berryman (2004a) were respectively, 0.005, 0.015, and 0.0125. Here we found that (β_1',β_3') for the same samples were, respectively, (0.05,0.90), (0.20,0.60), and (0.25,0.50). Clearly, these values are at least weakly correlated with those of the aspect ratios for the same samples, but no stronger conclusions can be reached at the present time concerning these values.

Similarly, the comparisons of the changes in shear modulus magnitude from drained to undrained also show a weak correlation. The increases in shear moduli observed in the measured laboratory data for Sierra White granite, Schuler-Cotton Valley sandstone, and Spirit River sandstone are, respectively, about 10%, 10%, and 20%. As seen in the TABLE, the magnitude of the changes predicted here is essentially about 10% in all three of these cases. Thus, agreement is good both qualitatively and semi-quantitatively in all cases. We conclude that the theory presented here is correctly predicting the magnitudes of these shear modulus enhancements due to pore-fluid effects.

6 Summary and Conclusions

The preceding discussion shows how overall shear modulus dependence on pore-fluid mechanics arises in simple anisotropic (the specific example used was transversely isotropic) media. The results — both the product formula derived previously by the author and the new formulas such as (35) — demonstrate in an entirely elementary fashion how compression-to-shear coupling enters the analysis for anisotropic materials, and furthermore how this coupling leads to overall shear dependence on mechanics of fluids in the pore system.

These effects need not always be large. However, the effect can be very substantial (on the order of a 10% to 20% increase in the overall shear modulus) in cracked or fractured materials, when these pores are liquid-filled. The anisotropy and liquid stiffening effects then both come strongly into play in the results we see, such as those illustrated in Figures 1–8. In particular, if $\beta_1 \simeq \beta_3$, then soft anisotropy does not make a significant contribution. But, if either $\beta_1 << \beta_3$ or $\beta_1 >> \beta_3$, then the contribution can be significant.

The results presented here are expected to be useful in reconciling high frequency shear wave data with the poroelastic theory and also as a tool for benchmarking of poroelastic codes for complex, heterogeneous earth systems such as reservoirs.

Acknowledgments

Work performed under the auspices of the U.S. Department of Energy under contract No. W-7405-ENG-48 and supported specifically by the Geosciences Research Program of the DOE Office of Basic Energy Sciences, Division of Chemical Sciences, Geosciences and Biosciences. Work also supported in part by the Stanford Exploration Project, while on sabbatical visiting the Geophysics Department at Stanford University.

Appendix A – Energy Ellipses

The equation of an ellipse centered at the origin whose semi-major and semi-minor axes are of lengths a and b and whose angle of rotation with respect to the x-axis in the (x, y)-plane is ψ is given by

$$(x\cos\psi + y\sin\psi)^2/a^2 + (-x\sin\psi + y\cos\psi)^2/b^2 = 1. \tag{37}$$

For comparison, when $x = r\cos\theta$, $y = r\sin\theta$, and a stress of magnitude $r = \sqrt{x^2 + y^2}$ is applied to a poroelastic system, the energy stored in the anisotropic media of interest here [using (16) and (18)] is given by

$$r^2 f^T(\theta)\Sigma^* f(\theta) \equiv U(r,\theta) = \\ 3r^2\left[A_{11}\cos^2\theta + 2\sqrt{2}A_{13}\cos\theta\sin\theta + 2A_{33}\sin^2\theta\right] = R^2 U(r_0,\theta). \tag{38}$$

In the second equation $R \equiv r/r_0$, and r_0 in an arbitrary number (say unity) having the dimensions of stress (*i.e.*, dimensions of Pa). It is not hard to see that, when $U(r,\theta) = const$, the two equations (37) and (38) have the same functional form and, therefore, that contours of constant energy in the complex $(z = x + iy)$ plane are ellipses. Furthermore, we can solve

for the parameters of the ellipse by setting $U = 1$ (in arbitrary units for now) in (38) and then factoring r^2 out of both equations. We find that

$$\begin{aligned} 3A_{11} &= \frac{\cos^2\psi}{a^2} + \frac{\sin^2\psi}{b^2}, \\ 6\sqrt{2}A_{13} &= \sin 2\psi \left(\frac{1}{a^2} - \frac{1}{b^2}\right), \\ 6A_{33} &= \frac{\sin^2\psi}{a^2} + \frac{\cos^2\psi}{b^2}. \end{aligned} \tag{39}$$

These three equations can be inverted for the parameters of the ellipse, giving:

$$\begin{aligned} \frac{1}{a^2} &= \frac{3A_{11}\cos^2\psi - 6A_{33}\sin^2\psi}{\cos 2\psi}, \\ \frac{1}{b^2} &= -\frac{3A_{11}\sin^2\psi - 6A_{33}\cos^2\psi}{\cos 2\psi}, \\ \tan 2\psi &= \frac{2\sqrt{2}A_{13}}{A_{11} - 2A_{33}}. \end{aligned} \tag{40}$$

Although contours of constant energy are of some interest, it is probably more useful to our intuition for the poroelastic application to think instead about contours associated with applied stresses and strains of unit magnitude, *i.e.*, for $r = 1$ (in appropriate units) and θ varying from 0 to π [again see definition (18)]. We then have the important function $U(1, \theta)$. [Note that, when θ varies instead between π and 2π, we just get a copy of the behavior for θ between 0 and π. The only difference is that the stress and strain vectors have an overall minus sign relative to those on the other half-circle. For a linear system, such an overall phase factor of unit magnitude is irrelevant to the mechanics of the problem.] Then, if we set $U(r, \theta) = const = R^2 U(r_0, \theta)$ and plot $z = Re^{i\theta}$ in the complex plane, we will have a plot of the ellipse of interest with R determined analytically by

$$R = \sqrt{U(r, \theta)/U(r_0, \theta)} = \sqrt{const/U(r_0, \theta)}. \tag{41}$$

We call R the magnitude of the normalized stress (*i.e.*, normalized with respect to r_0).

The analysis just outlined can then be repeated for the stiffness matrix and applied strain vectors. The mathematics is completely analogous to the case already discussed, so we will not repeat it here. Since strain is already a dimensionless quantity, the factor that plays the same role as r_0 above can in this case be chosen to be unity if desired, as the main purpose of the factor r_0 above was to keep track of the dimensions of the stress components.

Appendix B – Proof of the Product Formula

The product formula (32) was first presented in Berryman (2004a), where a couple of derivations of this formula were also given. A new derivation is provided here.

Using the definitions of unit trial vector f and reduced (*i.e.*, 2×2) compliance matrix Σ^* from Eqs. (18) and (16), we can immediately write the eigenvalue (or singular value) decomposition of the matrix Σ^* in terms of its eigenvectors and eigenvalues $f(\theta_\pm)$ and $\Lambda_\pm$. The result is

$$\Sigma^* = f(\theta_+)\Lambda_+ f^T(\theta_+) + f(\theta_-)\Lambda_- f^T(\theta_-). \tag{42}$$

The reduced stiffness matrix is just the inverse of Σ^*, and so is represented similarly by

$$(\Sigma^*)^{-1} = f(\theta_+)\Lambda_+^{-1} f^T(\theta_+) + f(\theta_-)\Lambda_-^{-1} f^T(\theta_-). \tag{43}$$

The curves in the Figures here can then all be parametrized in terms of polar angle θ by considering the formulas

$$f^T(\theta)\Sigma^* f(\theta) = \Lambda_+ \cos^2(\theta - \theta_+) + \Lambda_- \cos^2(\theta - \theta_-) \tag{44}$$

for compliance, and

$$f^T(\theta)\,(\Sigma^*)^{-1}\,f(\theta) = (\Lambda_+)^{-1}\cos^2(\theta - \theta_+) + (\Lambda_-)^{-1}\cos^2(\theta - \theta_-) \tag{45}$$

for stiffness.

Then, the undrained bulk modulus of the system $K_u = K_R$ is found from (42) to be

$$(3K_R)^{-1} = \overline{v}_1^T \Sigma^* \overline{v}_1 = \Lambda_+ \cos^2\theta_+ + \Lambda_- \cos^2\theta_-. \tag{46}$$

Similarly, the effective undrained shear modulus G_{eff} by definition is determined from

$$2G_{eff} = \overline{v}_3^T\,(\Sigma^*)^{-1}\,\overline{v}_3 = \Lambda_+^{-1}\sin^2\theta_+ + \Lambda_-^{-1}\sin^2\theta_-. \tag{47}$$

Taking the ratio of these quantities of interest, we find easily that

$$\frac{1}{6K_R G_{eff}} = \frac{\Lambda_+\cos^2\theta_+ + \Lambda_-\cos^2\theta_-}{\Lambda_+^{-1}\sin^2\theta_+ + \Lambda_-^{-1}\sin^2\theta_-} = \Lambda_+\Lambda_-, \tag{48}$$

where the final equality follows directly from the identity

$$\sin^2\theta_- = \sin^2\left(\theta_+ + \frac{\pi}{2}\right) = \cos^2\theta_+. \tag{49}$$

Eq. (48) is a special case of a more general product formula, true for any angle θ, which follows from the identity

$$\begin{aligned} f^T(\theta)\Sigma^* f(\theta)/\sqrt{\Lambda_+\Lambda_-} &= \sqrt{\frac{\Lambda_+}{\Lambda_-}}\cos^2(\theta-\theta_+) + \sqrt{\frac{\Lambda_-}{\Lambda_+}}\cos^2(\theta-\theta_-) \\ &= f^T(\theta+\pi/2)\,(\Sigma^*)^{-1}\,f(\theta+\pi/2)/\sqrt{\Lambda_+^{-1}\Lambda_-^{-1}} \end{aligned} \tag{50}$$

and is straighforward to verify.

Equation (48) is the product formula quoted in equation (32), and first derived in Berryman (2004a). A geometrical interpretation of the formula is obtained by considering, for example, Figure 1. A plane rectangle is formed by considering the origin and the two points labeled by $(\Lambda_+)^{-1}$ and $(\Lambda_-)^{-1}$ to be three of the four vertices of this rectangle. The area of this rectangle is clearly the product $(\Lambda_+\Lambda_-)^{-1}$. Similarly, the plane rectangle formed in the same way from the origin and the points labeled $2G_{eff}$ and $3K_R$ clearly has area $6G_{eff}K_R$. It is seen in Figure 1 that, at least to graphical accuracy, these two rectangles are practically indistinguishable — although in fact they are not identical. Formula (48) shows further that the areas of these two rectangles are always equal. A similar discussion also applies to the inverses of these quantities as demonstrated in Figure 8.

References

Backus, G. E. (1962) Long-wave elastic anisotropy produced by horizontal layering. *J. Geophys. Res.* **67**, 4427–4440.

Berge, P. A., and Berryman, J. G. (1995) Realizability of negative pore compressibility in poroelastic composites. *ASME J. Appl. Mech.* **62**, 1053–1062.

Berryman, J. G. (1999) Origin of Gassmann's equations. *Geophysics* **64**, 1627–1629.

Berryman, J. G. (2004a) Poroelastic shear modulus dependence on pore-fluid properties arising in a model of thin isotropic layers. *Geophys. J. Int.* **157**, 415–425.

Berryman, J. G. (2004b) Modeling high-frequency acoustic velocities in patchy and partially saturated porous rock using differential effective medium theory. *Int. J. Multiscale Computational Engineering*, in press.

Berryman, J. G. (2004c) Elastic and poroelastic analysis of Thomsen parameters for seismic waves in finely layered VTI media. submitted to *Geophysics*, currently under review.

Berryman, J. G., Berge, P. A., and Bonner, B. P. (2002a) Estimating rock porosity and fluid saturation using only seismic velocities. *Geophysics* **67**, 391–404.

Berryman, J. G., Pride, S. R., and Wang. H. F. (2002b) A differential scheme for elastic properties of rocks with dry or saturated cracks. *Geophys. J. Int.* **151**, 597–611.

Berryman, J. G., and Thigpen, L. (1985) Nonlinear and semilinear dynamic poroelasticity with microstructure. *J. Mech. Phys. Solids* **33**, 97–116.

Berryman, J. G., and Wang, H. F. (2001) Dispersion in poroelastic systems. *Phys. Rev. E* **64**, 011303.

Biot, M. A. (1962a) Generalized theory of acoustic propagation in porous dissipative media. *J. Acoust. Soc. Am.* **34**, 1254–1264.

Biot, M. A. (1962b) Mechanics of deformation and acoustic propagation in porous media. *J. Appl. Phys.* **33**, 1482–1498.

Biot, M. A., and Willis, D. G. (1957) The elastic coefficients of the theory of consolidation. *J. Appl. Mech.* **24**, 594–601.

Bourbié, T., Coussy, O., and Zinszner, B. (1987) *Acoustics of Porous Media*. Gulf Publishing Company, Houston, pp. 85–95.

Brown, R. J. S., and Korringa, J. (1975) On the dependence of the elastic properties of a porous rock on the compressibility of a pore fluid. *Geophysics* **40**, 608–616.

Chin, R. C. Y., Berryman, J. G., Hedstrom, G. W. (1985) Generalized ray expansion for pulse propagation and attenuation in fluid-saturated porous media. *Wave Motion* **7**, 43–66.

Gassmann, F. (1951) Über die elastizität poröser medien. *Veirteljahrsschrift der Naturforschenden Gesellschaft in Zürich* **96**, 1–23.

Hudson, J. A. (1981) Wave speeds and attenuation of elastic waves in material containing cracks. *Geophys. J. R. Astr. Soc.* **64**, 133–150.

Knight, R., and Nolen-Hoeksema, R. (1990) A laboratory study of the dependence of elastic wave velocities on pore scale fluid distribution. *Geophys. Res. Lett.* **17**, 1529–1532.

Mavko, G., and Jizba, D. (1991) Estimating grain-scale fluid effects on velocity dispersion in rocks. *Geophysics* **56**, 1940–1949.

Mukerji, T., and Mavko, G. (1994) Pore fluid effects on seismic velocity in anisotropic rocks. *Geophysics* **59**, 233–244.

Murphy, William F., III (1982) *Effects of Microstructure and Pore Fluids on the Acoustic Properties of Granular Sedimentary Materials*, Ph.D. Dissertation, Stanford University.

Norris, A. N. (1993) Low-frequency dispersion and attenuation in partially saturated rocks. *J. Acoust. Soc. Am.* **94**, 359–370.

O'Connell, R. J., and Budiansky, B. (1974) Seismic velocities in dry and saturated cracked solids. *J. Geophys. Res.* **79**, 5412–5426.

Plona, T. J. (1980) Observation of a second bulk compressional wave in a porous medium at ultrasonic frequencies. *Appl. Phys. Lett.* **36**, 259–261.

Pride, S. R., Berryman, J. G., and Harris, J. M. (2004) Seismic attenuation due to wave induced flow. *J. Geophys. Res.* **109**, B01201.

Rice, J. R., and Cleary, M. P. (1976) Some basic stress diffusion solutions for fluid-saturated elastic porous media with compressible constituents. *Rev. Geophys.* **14**, 227–241.

Sams, M. S., Neep, J. P., Worthington, M. H., and King, M. S. (1997) The measurement of velocity dispersion and frequency-dependent intrinsic attenuation in sedimentary rocks. *Geophysics* **62**, 1456–1464.

Skempton, A. W. (1954) The pore-pressure coefficients A and B. *Geotechnique* **4**, 143–147.

Walsh, J. B. (1969) New analysis of attenuation in partially melted rock. *J. Geophys. Res.* **74**, 4333–4337.

Williams, K. L., Jackson, D. R., Thorsos, E. I., Tang, D., and Schock, S. G. (2002) Comparison of sound speed and attenuation measured in a sandy sediment to predictions based on the Biot theory of porous media. *IEEE J. Ocean. Eng.* **27**, 413–428.

TABLE. Elastic and poroelastic parameters of the three rock samples considered in the text. Bulk and shear moduli of the grains K_m and G_m, bulk and shear moduli of the drained porous frame K_{dr} and G_{dr}, the effective and undrained shear moduli G_{eff} and G_u, and the Biot-Willis parameter $\alpha = 1 - K_{dr}/K_m$. The porosity is ϕ.

Elastic/Poroelastic Parameters	Sierra White Granite	Schuler-Cotton Valley Sandstone	Spirit River Sandstone
G_m (GPa)	31.7	36.7	69.0
G_u (GPa)	28.3	17.7	12.41
G_{dr} (GPa)	26.4	15.7	11.33
G_{eff} (GPa)	39.8	35.8	20.11
K_m (GPa)	57.7	41.8	30.0
K_{dr} (GPa)	38.3	13.1	7.04
α	0.336	0.687	0.765
ϕ	0.008	0.033	0.052

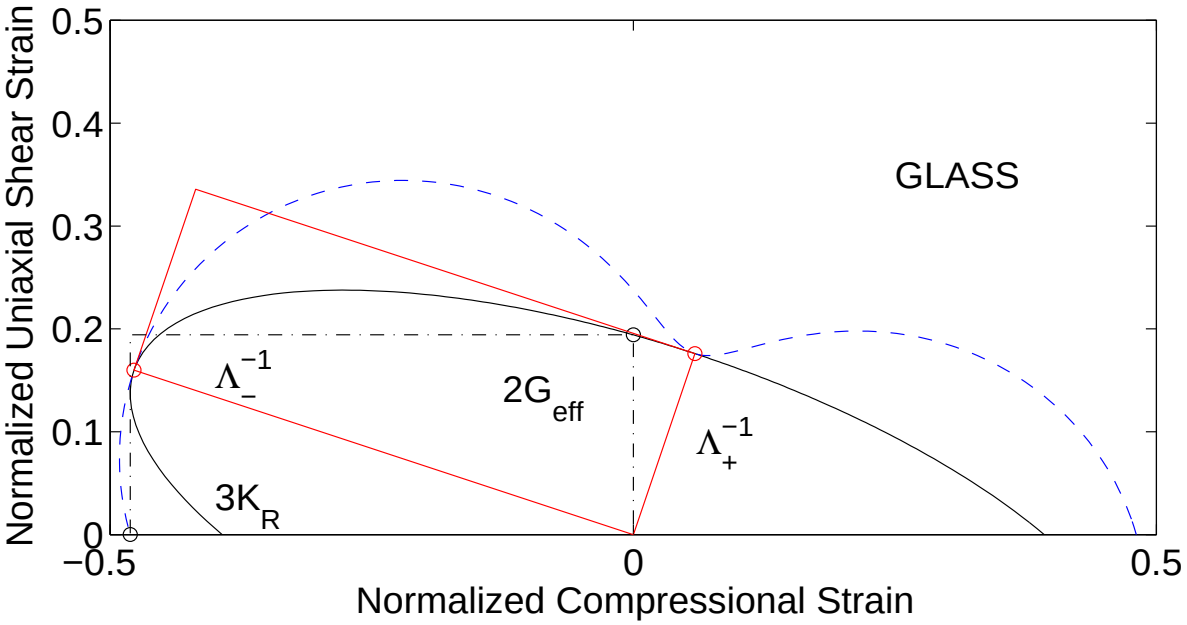

Figure 1: For a glassy porous material having bulk modulus $K_{dr} = 18.52$ GPa and shear modulus $G_{dr} = 13.89$ GPa, the locus of points $z = Re^{i\theta}$ [see equation (38)] having constant energy $U = 900$ GPa, when the linear combination of pure compression and pure uniaxial shear is interpreted as strain field applied to the stiffness matrix (solid black line). The plot is in the complex z-plane, with the inverse of the corresponding expression for the compliance energy superposed for comparison (dashed blue line). Red circles at the two points of intersection correspond to the two eigenvalues/eigenvectors of the system of equations. The ellipse (solid black line) in this plane corresponds to the more complex curve in Figure 2. The two rectangles illustrate the inverse of the product formula (32) derived and used in the text. The shapes of these rectangles are very similar, but not identical; however, their areas are identical.

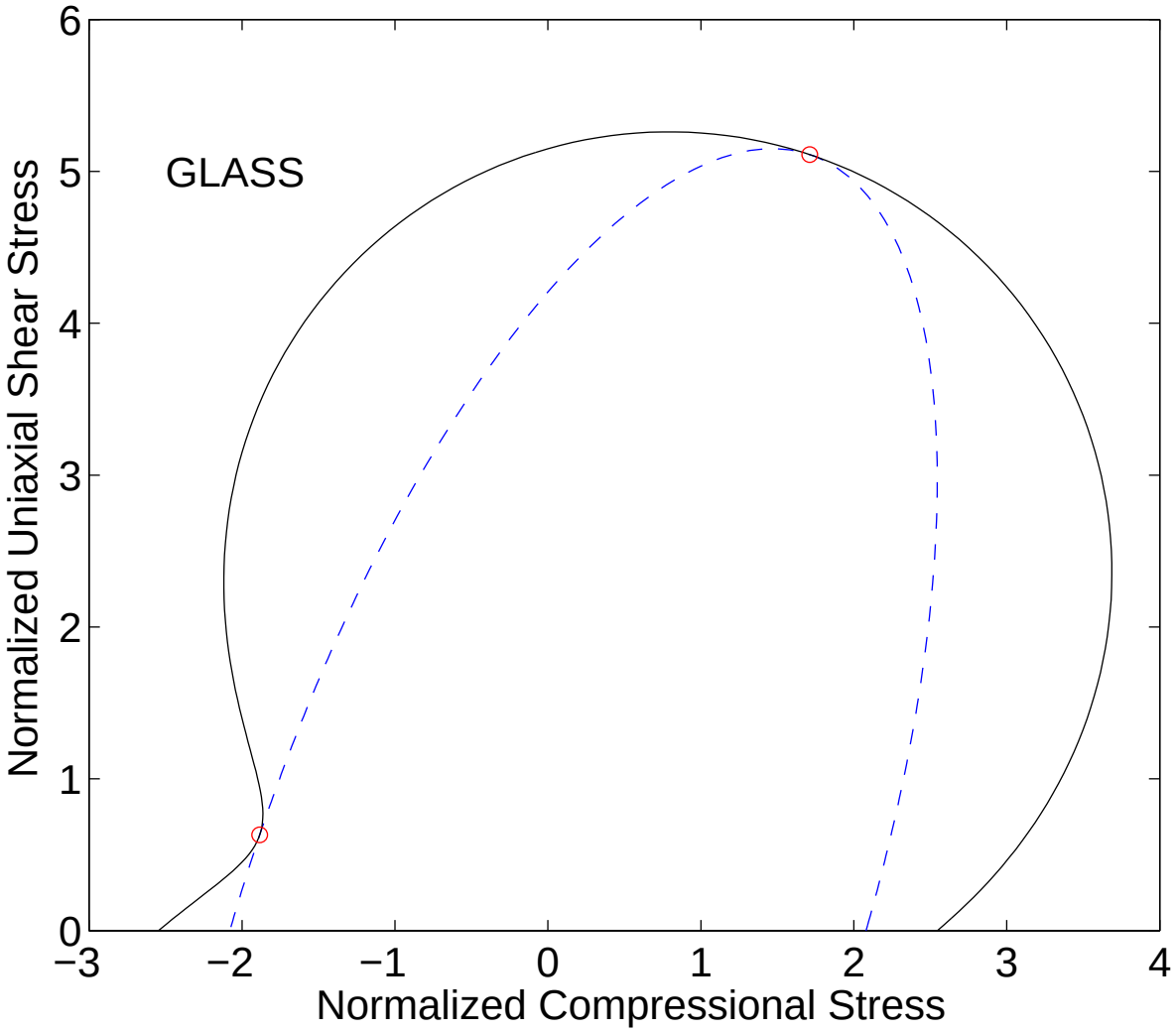

Figure 2: Same parameters as Figure 1, but the linear combination of pure compression and pure uniaxial shear is interpreted as a stress field and is applied to the compliance matrix (dashed blue line). The plot is again in the complex z-plane, with the inverse of the corresponding expression for the stiffness energy superposed for comparison (solid black line). Red circles at the two points of intersection correspond to the two eigenvalues/eigenvectors of the system of equations. The ellipse (dashed blue line here) corresponds to the more complex curve in Figure 1.

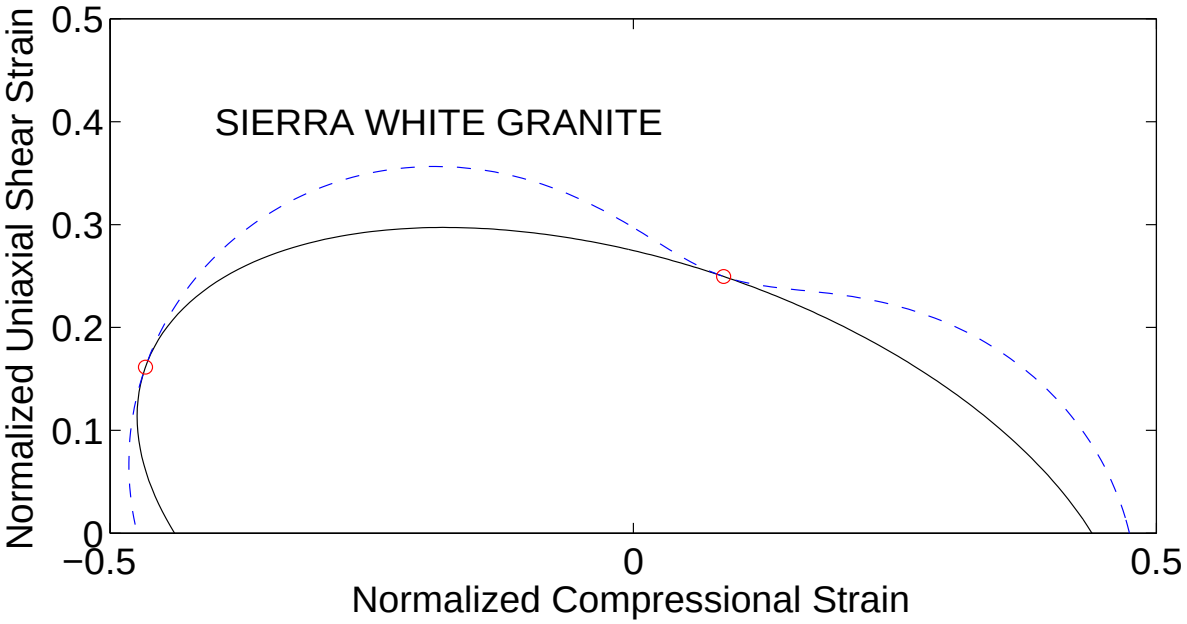

Figure 3: Same as Figure 1 for Sierra White Granite using the parameters from the TABLE.

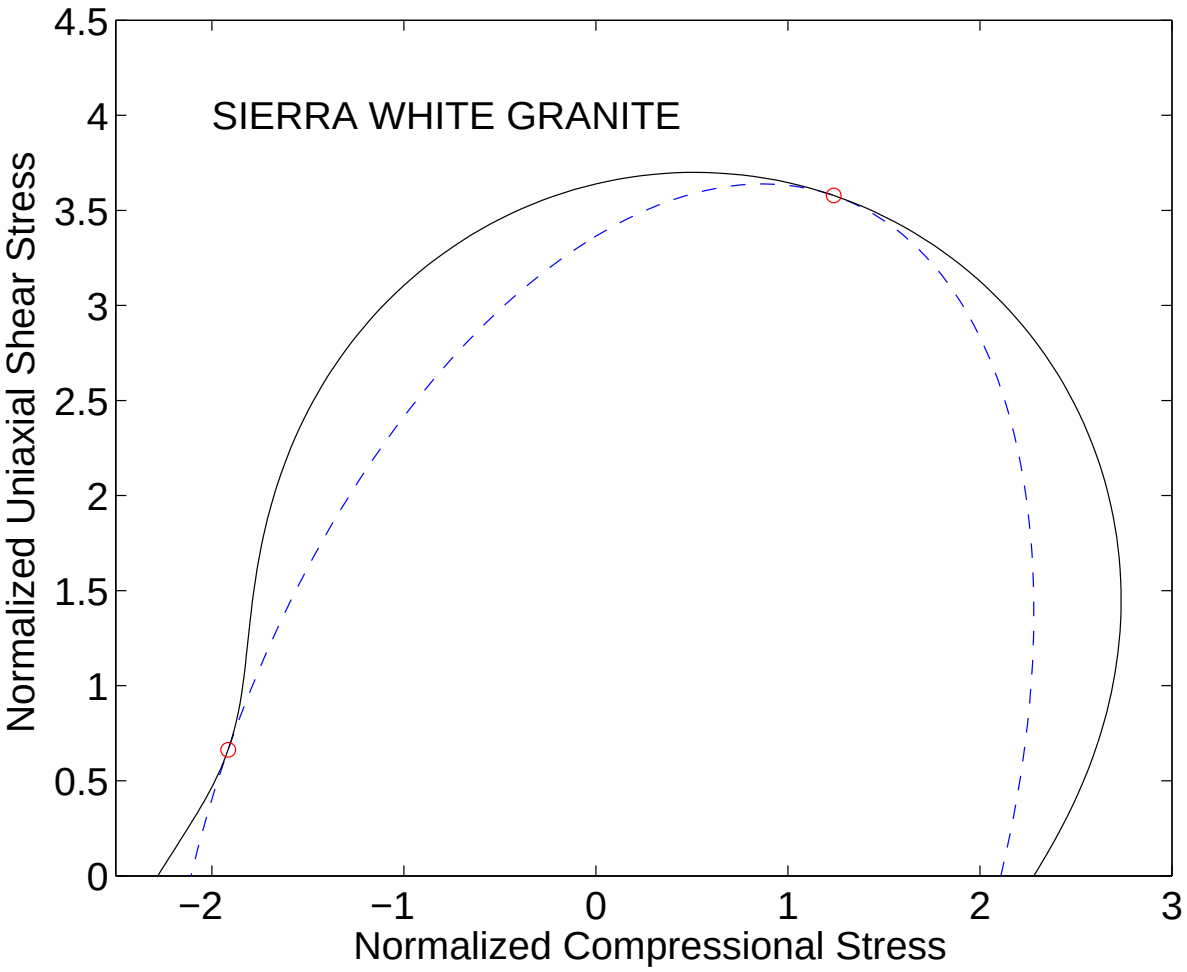

Figure 4: Same as Figure 2 for Sierra White Granite using the parameters from the TABLE.

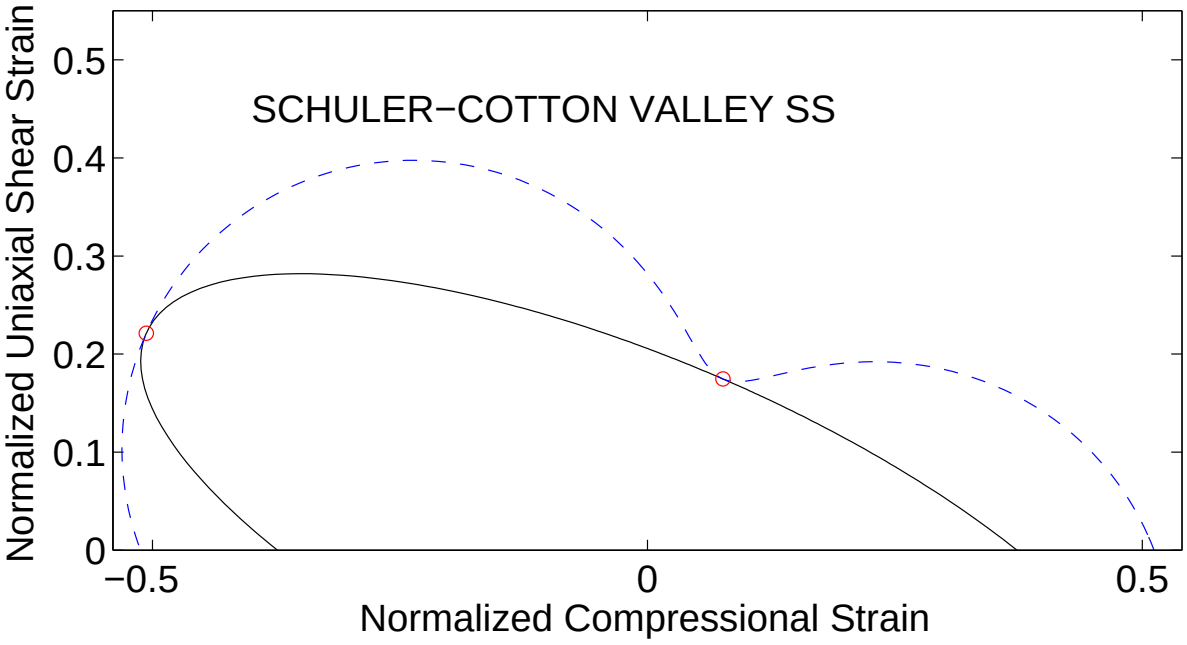

Figure 5: Same as Figure 1 for Schuler-Cotton Valley Sandstone using the parameters from the TABLE.

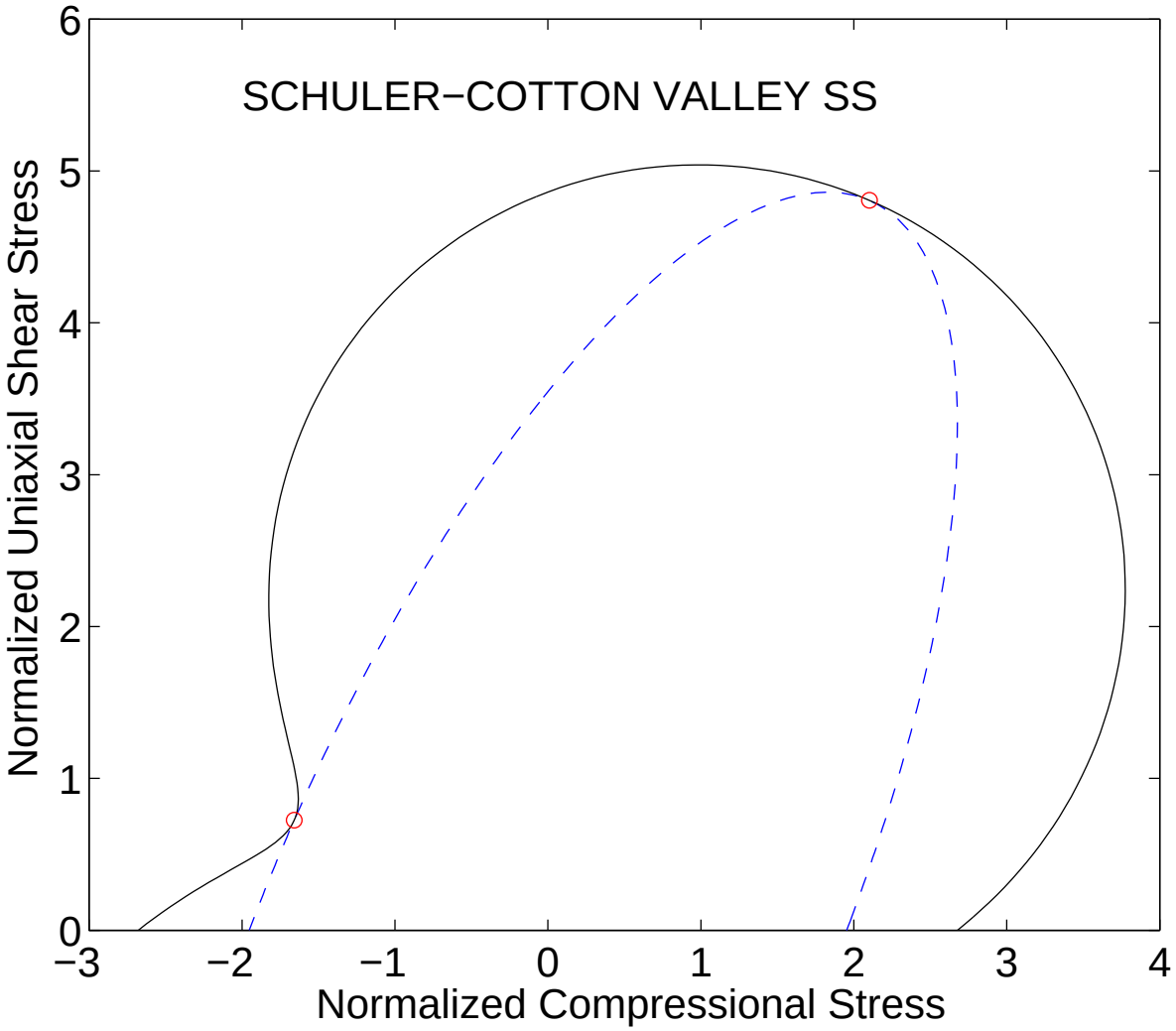

Figure 6: Same as Figure 2 for Schuler-Cotton Valley Sandstone using the parameters from the TABLE.

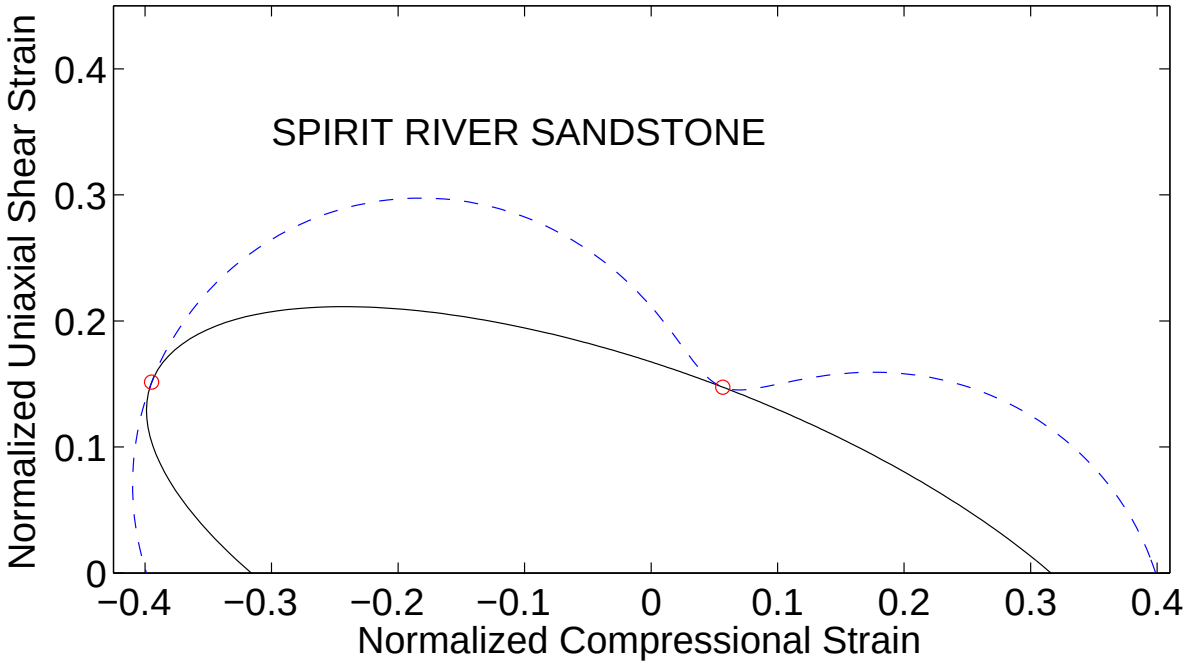

Figure 7: Same as Figure 1 for Spirit River Sandstone using the parameters from the TABLE.

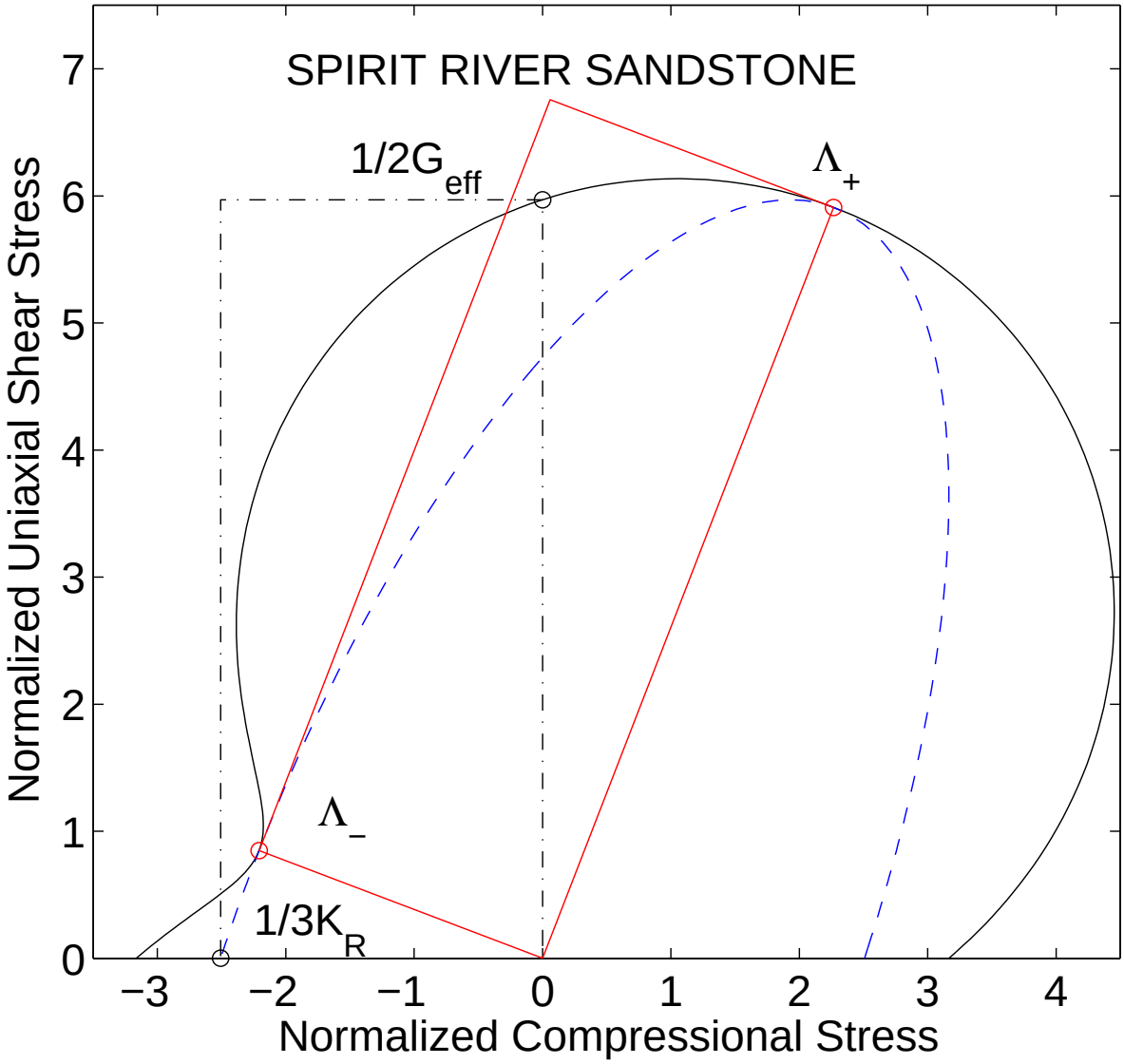

Figure 8: Same as Figure 2 for Spirit River Sandstone using the parameters from the TABLE. The two rectangles illustrate the product formula (32) derived and used in the text. The shapes of these rectangles are very similar, but not identical; however, their areas are identical.